Numerical modeling of spalling brittle fracture along the (0001) plane in HCP-single crystals under shock loading

M. N. Krivosheina, E. V. Tuch, and S. V. Kobenko

Citation: AIP Conference Proceedings **2051**, 020152 (2018); doi: 10.1063/1.5083395
View online: https://doi.org/10.1063/1.5083395
View Table of Contents: http://aip.scitation.org/toc/apc/2051/1
Published by the American Institute of Physics

Numerical Modeling of Spalling Brittle Fracture along the (0001) Plane in HCP-Single Crystals under Shock Loading

M. N. Krivosheina[1,2,a)], E. V. Tuch[1,b)], and S. V. Kobenko[3,c)]

[1] *Institute of Strength Physics and Materials Science SB RAS, Tomsk, 634055 Russia*
[2] *National Research Tomsk State University, Tomsk, 634050 Russia*
[3] *Nizhnevartovsk State University, Nizhnevartovsk, 628605 Russia*

[a)] marina_nkr@mail.ru
[b)] Corresponding author: tychka2012@mail.ru
[c)] sergeyvk@inbox.ru

Abstract. Numerical modeling of spalling brittle fracture along the (0001) plane in a zinc single crystal under shock loading by an aluminum projectile was performed in the work. Numerical modeling was carried out by the finite element method in a three-dimensional statement. The mathematical model allows to take into account the anisotropy of bulk compressibility in a single crystal of zinc, auxeticity, anisotropy of the propagation velocities of elastic longitudinal and volume waves. Stresses are determined on the basis of a comparison of velocity profiles of the rear surfaces of targets from zinc single crystal in mutually perpendicular directions when it is destroyed along the (0001) plane in natural experiments and numerical simulation.

INTRODUCTION

Now, the main method for studying the propagation of elastoplastic waves in materials characterized by transversally isotropic elastic, plastic and strength properties is the natural experiment [1–12]. In this case in processing the results of natural experiments various mathematical models can be used. For example, mathematical model which is used in processing of natural experiments can have the hypothesis about the compliance of volume strain to hydrostatic stress or about the compliance to anisotropic pressure. In one-dimensional experiments in the direction of shock loading a one-dimensional deformation processes realized, therefore in mathematical models only one value of the Poisson coefficient is used in processing the results of natural experiments. In transversely isotropic materials, there are always three different Poisson's ratios, including those that sometimes have negative values. Investigations of deformation processes using numerical modeling make it possible to distinguish the contribution of anisotropy of elastic, plastic and strength properties to the final picture of the destruction of such materials. The analysis of the propagation of elastoplastic waves was carried out using numerical modeling in transversally isotropic materials using a mathematical model within the framework of the hypothesis of bulk anisotropy of deformation processes in the proposed work. Numerical modeling of spall destruction of targets from transversally isotropic materials using the example of zinc single crystal was carried out by the finite element method in a three-dimensional statement. The results of numerical modeling are compared with the experimental data [13] on the shock load of a zinc single crystal in the [0001] direction. The velocities of propagation of elastic longitudinal and volume waves in this direction in a target from a single crystal of zinc have close values, and therefore it is impossible to fix the branches of the elastic precursor from the plastic compression wave when they exit the rear surface of the target in natural experiments. In numerical calculations, it is also impossible to isolate the yield of an elastic precursor on the rear surface of the target in the [0001] direction, but obtaining an analogous profile of the velocity of the rear surface of the target makes it possible to determine the values of the dynamic yield strength and spalling strength of the target material.

Proceedings of the Advanced Materials with Hierarchical Structure for New Technologies and Reliable Structures
AIP Conf. Proc. 2051, 020152-1–020152-5; https://doi.org/10.1063/1.5083395
Published by AIP Publishing. 978-0-7354-1777-9/$30.00

MATHEMATICAL MODEL OF BRITTLE FRACTURE OF A MATERIAL WITH A TRANSVERSELY ISOTROPIC SYMMETRY OF PROPERTIES

The system of equations describing the non-stationary adiabatic motions of the compressible anisotropic medium includes [14] equation of continuity:

$$\frac{\mathrm{d}\rho}{\mathrm{d}t} + \rho \operatorname{div}\mathbf{v} = 0, \tag{1}$$

motion equation

$$\rho \frac{\mathrm{d}v_k}{\mathrm{d}t} = \frac{\partial \sigma_{ki}}{\partial x_i} + F_k, \tag{2}$$

energy equation

$$\frac{\mathrm{d}E}{\mathrm{d}t} = \frac{1}{\rho}\sigma_{ij} e_{ij}, \tag{3}$$

where ρ—medium density, $\mathbf{v}$—velocity vector, F_k—components of the body force vector, σ_{ij}—components of symmetric stress tensor, E—specific internal energy, e_{ij}—components of symmetric strain velocity tensor:

$$e_{ij} = \frac{1}{2}(\nabla_i v_j + \nabla_j v_i), \tag{4}$$

v_i—components of velocity vector, $i, j = 1, 2, 3$.

The total stress tensor is decomposed into deviatoric stress and anisotropic hydrostatic stress [15]:

$$\sigma_{ij} = S_{ij} - P_e \lambda_{ij}, \tag{5}$$

where S_{ij} are the components of the total stress deviator, λ_{ij} is the generalized Kronecker delta, P_e is the spherical part of the total stress tensor. In the elastic range

$$S_{ij} = C_{ijkl}\varepsilon_{kl}, \quad \lambda_{ij} = \frac{C_{ijkl}\delta_{kl}}{3K_a}, \quad K_a = \frac{1}{9}C_{ijkl}\delta_{ij}\delta_{kl}, \quad P_e = \frac{\varepsilon_V C_{ijkl}\delta_{ij}\delta_{kl}}{3},$$

where K_a is the generalized bulk modulus, δ_{kl} is the Kronecker-delta, ε_{kl} are the strain deviator components, C_{ijkl} are elastic constants, ε_V is the volume strain for an anisotropic medium.

In the elastic range, the decomposition of total stress tensor (5) is equivalent to calculations in terms of total stress.

In the plastic range, the pressure P_e for an anisotropic material is estimated by the Mie–Grüneisen equation as a function of specific internal energy E and current density:

$$P_e = \sum_{n=1}^{3} K_n \left(\frac{V}{V_0} - 1\right)^n \left[1 - K_0\left(\frac{V_0}{V} - 1\right)\Big/ 2\right] + K_0 \rho E, \tag{6}$$

where K_0, K_1, K_2, K_3 are material constants, V, V_0 are the current and initial volumes.

The total stress in the plastic range is also estimated by formula (5). The components of the total stress deviator are calculated according to the flow theory. The plastic strain is estimated using the non-associated flow rule:

$$\mathrm{d}\varepsilon_{ij}^{\mathrm{p}} = \mathrm{d}\lambda \frac{\partial F}{\partial \sigma_{ij}} \tag{7}$$

with $\mathrm{d}\lambda$ being zero in the elastic range and always positive in the plastic range (yield criterion), $\varepsilon^{\mathrm{p}}{}_{ij}$ are the plastic strain components; and F is the yield function.

The von Mises–Hill criterion (1948) in terms of stress deviators for transversally isotropic materials with regard to isotropic hardening has the form

$$F(S_{ij}, R) = \frac{S_{11}^2}{r_1^2} + \frac{S_{22}^2}{r_2^2} + \frac{S_{33}^2}{r_3^2} + \frac{S_{12}^2}{r_4^2} + \frac{S_{31}^2}{r_5^2} + \frac{S_{23}^2}{r_6^2} - R^2 = 0, \tag{8}$$

where r_i is determined in terms of tensile and shear yield strengths for a transversally isotropic material, R is the isotropic hardening function. As has been shown [16], the function R is the invariant with respect to stress state. It is defined for a simple form of loading and depends linearly on the accumulated plastic strain ε^{p}:

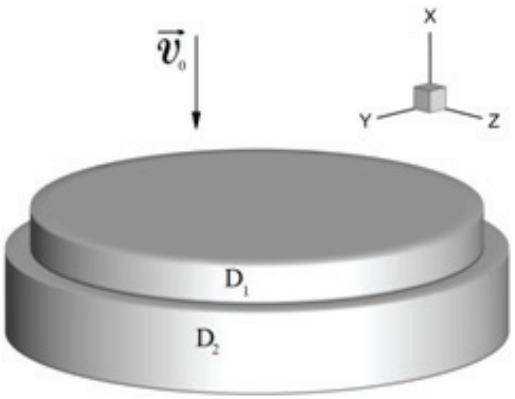

FIGURE 1. Initial configuration of projectile and target

$$R(\varepsilon^{\mathrm{p}}) = 1 + \xi\varepsilon^{\mathrm{p}}, \tag{9}$$

where $\varepsilon^{\mathrm{p}} = \int \left| \mathrm{d}\,\varepsilon^{\mathrm{p}}_{kl} \right|$, $k, l = 1, ..., 3$.

The elastoplastic deformation of an isotropic material (impactor) is described using the Prandtl–Reuss model. Brittle fracture of the target is modeled by the Hoffman failure criterion, which allows for anisotropy of the tensile and shear strength characteristics [17]

$$\begin{aligned} &C_1(\sigma_{22} - \sigma_{33})^2 + C_2(\sigma_{33} - \sigma_{11})^2 + C_3(\sigma_{11} - \sigma_{22})^2 \\ &+ C_4\sigma_{11} + C_5\sigma_{22} + C_6\sigma_{33} + C_7\sigma_{12}^2 + C_8\sigma_{23}^2 + C_9\sigma_{31}^2 \geq 1 \end{aligned} \tag{10}$$

The stresses in an element rigidly rotated in space are reduced through the Jaumann derivative to the coordinate system

$$\frac{\mathrm{D}\sigma_{ij}}{\mathrm{D}t} = \frac{\mathrm{d}\sigma_{ij}}{\mathrm{d}t} - \sigma_{ik}\omega_{jk} - \sigma_{jk}\omega_{ik}, \text{ where } \omega_{ij} = \frac{1}{2}\left(\frac{\partial v_j}{\partial x_i} - \frac{\partial v_i}{\partial x_j} \right).$$

PROBLEM STATEMENTS FOR SHOCK-LOADED TARGET OF SINGLE CRYSTALS OF ZINC

The problem statement for our 3D finite element simulation of impacted single crystals of zinc was the same as in experiments [13]. The elastic constants of the transversally isotropic zinc target were the following [13] (see table).

The modeling was performed using original software. Figure 1 shows the initial configuration of the projectile (25 920 tetrahedrons) and target (227 430 tetrahedrons). The initial velocity of Al projectile V_0 = 650 m/s, thickness of the projectiles are in first case 0.85 mm, in second 0.4 mm, thickness of the target 1.7 mm.

The profiles of the speed of the surface of sample of zinc single crystal under loading in the [0001] direction obtained in [13] are shown in Fig. 2. The lower curve corresponds to the thickness of the projectile 0.4 mm, the upper one 0.85 mm. The curves were compared with the velocity profiles of the free surfaces of samples of single crystals of zinc obtained in numerical simulations (Fig. 3). If we compare the profiles of the curves, we can see that for both thicknesses of the projectiles the maximum and minimum values of the speeds of rear surfaces of zinc single crystal coincide. The values of the reflection times from the rear surface of the targets of the compression waves coincide as well.

TABLE 1

C_{11}, MPa	C_{33}, MPa	C_{12}, MPa	C_{23}, MPa	C_{44}, MPa
61041.7	161018.1	49987.7	45126.2	63445.9

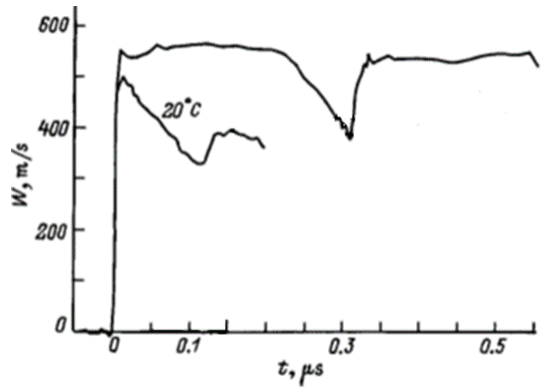

FIGURE 2. The velocity profiles of free surfaces of samples of single crystals of zinc under loading in the [0001] direction by shock of aluminum plates with thicknesses of 0.4 mm and 0.85 mm at a velocity of 650–700 m/s [13]

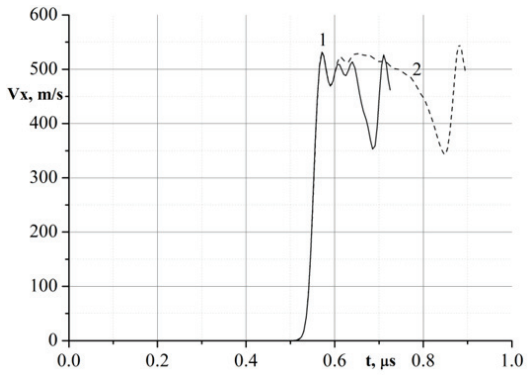

FIGURE 3. Calculated velocity profiles of free surfaces of samples of zinc single crystals under loading in the [0001] direction by shock of aluminum plates 0.4 mm thick (*1*) and 0.85 mm (*2*) at a velocity of 650 m/s

The following plastic and strength properties were calculated on the basis of the coincidence of the velocity profiles of the free surface of samples of zinc single crystals under loading in the [0001] direction: in the direction of [0001] the dynamic yield strength is $\sigma_d^{(0001)}$ = 3500 MPa, the spall strength is $\sigma_*^{(0001)}$ = 9000 MPa, in the perpendicular direction: $\sigma_d^{10\bar{1}0}$ = 1800 MPa, $\sigma_*^{10\bar{1}0}$ = 15 000 MPa. Dynamic yield stresses in mutually perpendicular directions are common for a zinc single crystal and do not depend on the type of the fracture. The calculated strength characteristics in mutually perpendicular directions are realized only when the zinc single crystal is spalled along the [0001] direction. The strength properties of a zinc single crystal will be different, since another mechanism of spall destruction is realized when shock loading along the $[10\bar{1}0]$ direction.

In the work within the framework of a mathematical model that allows to take into account the dependence of different propagation velocities of elastic longitudinal and plastic waves on the direction, velocity profiles of the rear surface of the target are obtained, which coincide with the profiles obtained in natural experiments [13]. As well as in natural experiments, there is no decomposition of the compression shock wave into an elastic precursor and a plastic compression wave. In the calculations, the elastic properties of a zinc single crystal were used from [13], the dynamic yield stresses and the strength limits for brittle spall fracture in the [0001] direction were obtained on the basis of the coincidence of the velocity profiles of the rear obstacle surfaces in calculations and natural experiments [13]. It is necessary to know the plastic properties in a direction perpendicular to the [0001] direction, to simulate spall fracture of the target in the [0001] direction. The dynamic yield strengths in the $[10\bar{1}0]$ direction were determined on the basis of the coincidence of the velocity profiles of the rear surfaces of the target from the zinc single crystal under shock loading in the $[10\bar{1}0]$ direction, as well as in [1], and in numerical calculations of the authors.

CONCLUSION

For the case of close values of the propagation velocities of longitudinal and volume waves and the separation of a shock wave into an elastic precursor and a plastic compression wave for this reason, the plastic and strength properties of a zinc single crystal with its brittle spall fracture in the (0001) plane are determined with the help of numerical modeling.

ACKNOWLEDGMENTS

This study was funded by Fundamental Research Program of State Academies of Sciences for 2013–2020 projects No. 23.1.2 and by RFBR according to the research project No. 18-31-00278 mol_a.

REFERENCES

1. N. Djordjevic, R. Vignjevic, L. Kiely, S. Case, T. De Vuyst, J. Campbell, and K. Hughes, Int. J. Plast. **105**, 211–224 (2018).
2. S. A. Habib, A. S. Khan, T. Gnäupel-Herold, and J. T. Lloyd, Int. J. Plast. **95**, 163–190 (2017).
3. S. Koubaa, J. Mars, M. WaliD, and F. Dammak, Int. J. Imp. Eng. **101**, 105–114 (2017).
4. A. E. Mayer, K. V. Khishchenko, P. R. Levashov, and P. N. Mayer, J. Appl. Phys. **113**, 193508 (2013).
5. J. Aboudi, Int. J. Solids Struct. **48**, 2102–2119 (2011).
6. J. Cao, F. Li, X. Ma, and Z. Sun, Int. J. Mech. Sci. **128-129**, 445–458 (2017).
7. L. Yoon, Key Eng. Mater. **163**(8), 651–653 (2015).
8. W. Liu, J. Manuf. Sci. Technol. **14**, 43–54 (2016).
9. A. Abd El-Aty, Y. Xu, S. H. Zhang, Y. Ma, and D. Y. Chen, Proc. Eng. **207**, 13–18 (2017).
10. S. Betsofen, V. Antipov, and M. Knyazev, Russ. Metall. **4**, 326–341 (2016).
11. J. Galicki and M. Czech, Appl. Math. Model. **37**, 815–827 (2013).
12. J. D. Seidt, J. M. Pereira, A. Gilat, D. M. Revilock, and K. Nandwana, Int. J. Imp. Eng. **62**, 27–34 (2013).
13. A. A. Bogach, G. I. Kanel, S. V. Razorenov, and A. V. Utkin, Phys. Solid State **40**, 1676–1680 (1998).
14. L. I. Sedov, *Continuum Mechanics* (Nauka, Moscow, 1976).
15. A. A. Lykianov and V. B. Penkov, Appl. Math. Mech. **73**(4), 635–644 (2009).
16. V. V. Kosarchuk, B. I. Kovalchuk, and A. A. Lebedev, Probl. Prochn. **4**, 50–56 (1986).
17. S. W. Tsai and E. M. Wu, J. Compos. Mater. **5**, 58–80 (1971).